

Eine Particle Image Velocimetry Untersuchung von Strömungen mit moderater Reynoldszahl in einem T-Mixer

A particle imaging velocimetry investigation of moderate Reynolds number flow in a T-mixer

Huixin Li¹, Duo Xu^{1,2}, Bastian Bäuerlein^{4,5}, Kerstin Avila^{4,5} and Marc Avila^{1,3}

1. Center of Applied Space Technology and Microgravity (ZARM), University of Bremen, Bremen, 28359, Germany

2. The State Key Laboratory of Nonlinear Mechanics, Institute of Mechanics, Chinese Academy of Sciences, Beijing, 100190, China

3. MAPEX Center for Materials and Processes, University of Bremen, Bremen, 28359, Germany

4. Particles and Process Engineering, University of Bremen, Bremen, 28359, Germany

5. Leibniz Institute for Materials Engineering IWT, Badgasteiner Strasse 3, Bremen, 28359, Germany

Email: huixin.li@zarm.uni-bremen.de

Keywords: T-mixer, PIV, Steady flows, Periodic flows

Abstract

In chemical and process engineering, mixing devices are used to study fluid mixing and its impact on chemical reactions. Among a variety of choices, T-shaped mixers have been widely used for fundamental studies because they are easy to fabricate and characterize with optical measurement methods. In this study, a T-shaped mixer was built with a height, H , of 4 centimetres to enable accurate measurements of small-scale mixing with optical techniques. In addition, long inlet channels ensure fully developed inflows and thus boundary conditions for comparisons with numerical simulations. We examine the fully developed laminar flows and repeat the flow regimes (e.g., the engulfment and the unsteady symmetric regimes) with particle imaging velocimetry (PIV) for different Reynolds numbers. The Strouhal number of the unsteady flows is cross-validated with numerical simulations. Overall, the present setup can achieve the inlets with fully developed laminar flows when $Re \leq 1100$ and repeat the flow regimes in previous studies.

Introduction

Fluid mixing is not only a fundamental and multi-scale process in engineering applications (e.g. in chemical and aerospace engineering), but is also ubiquitous in nature (e.g. atmospheric boundary layer and ocean flows). In chemical (process) engineering, micromixing devices are used to study the mixing process and their impact on (chemical) reactions. Due to the simple fabrication and good mixing efficiency, the T-mixer geometry has been widely used among a variety of micromixers. Thus, a number of studies pay attention to the T-mixer, revealing the physics of the mixing process, characterizing the mixing performance, and quantifying the quality of the mixing outcomes (Camarri et al. 2020).

The Reynolds number is the most important parameter determining the flow in a T-mixer. It is usually defined as $Re = U_0 H / \nu$, where U_0 is the mean velocity in the inlet channel, ν is the kinematic viscosity and H is the hydraulic diameter of the mixing channel. With the increase of

the Reynolds numbers in the T-mixer, different flow regimes have been broadly identified in previous numerical and experimental studies: the steady symmetric flow, engulfment flows (i.e., steady asymmetric flow and periodic asymmetric flow), the unsteady symmetric flow, and the chaotic flow (Camarri et al. 2020; Zhang et al. 2019; Fani et al. 2013 & 2014; Thomas and Ameel. 2010). When the Reynolds number is small ($Re \lesssim 105$), the steady and symmetric flow is dominant. Two parallel streams of fluid form and flow from the inlet channels to the mixing channel (Schikarski et al. 2017; Thomas and Ameel. 2010). As the Reynolds number increases, the symmetric flow state becomes unstable and is replaced by the engulfment flow state, which has been observed with planar laser-induced fluorescence (PLIF) (Hoffmann et al. 2006; Thomas and Ameel. 2010) and flow simulation (Fani et al. 2013, Schikarski et al. 2017). To identify the critical Re at which the transition from symmetric flow to engulfment flow occurs, Soleymani et al. (2008) provided an expression based on the numerical study, combined with the mixing channel length and aspect ratio of the T-mixers. Their expression was found to be consistent with experimental data for different T-mixers in the literature. Furthermore, through simulation and experiments, Cherlo and Pushpavanam (2010) and Poole et al. (2013) further confirmed this expression for predicting the critical Reynolds, but they found that the prediction of the expression failed when the height of the T-mixer was greater than the width.

In the engulfment regime, reflection symmetries are broken and the shear layer in the T junction starts to engulf both flow streams. Two vortexes are observed, which retain a central symmetry. The resulting enhancement of the mixing process has been discussed in several studies (Zhang et al. 2019; Fani et al. 2013 & 2014; Thomas and Ameel. 2010). At low Reynolds number, the engulfment flow is steady flow and later becomes unsteady (periodic) and chaotic (Schikarski et al. 2017). A transition Reynolds number from steady flow to unsteady engulfment flow was also reported in the literature, e.g., $Re \approx 142$ (Thomas and Ameel. 2010; Thomas et al. 2010; Engler et al. 2004), or $Re = 180 - 195$ (Zhang et al. 2019). Fani et al. (2013 & 2014) analysed the instability mechanism and precisely determined this critical Reynolds number ($Re \approx 175$) through the direct numerical simulation. The difference of these critical Reynolds numbers mentioned above might come from different aspect ratios of the setups. With further increasing Reynolds numbers ($\gtrsim 320$), the flow begins to regain symmetry but exhibits unsteady flow behaviour. At the same time, the mixing efficiency decreases. The flow pattern exhibits quasi-periodic behaviours for symmetric unsteady flow, in which oscillatory stagnation point behaviour is unpredictably interrupted by asymmetrical breaks (Thomas and Ameel. 2010). Periodic breaks from the symmetry that occur in this regime are more frequent with increasing Re , as the momentum field of the inlet flow in the T-mixer becomes increasingly more energetic. Subsequently, the flow regime becomes chaotic with the increase of the Reynolds number. When the Reynolds number is beyond 650, the flow in the mixing channel becomes eventually turbulent (Schikarski et al. 2019). However, only a few studies focused on the flow and mixing dynamics at high Reynolds numbers (> 500) for a T-mixer, especially through experiments. Thus, for the accurate measurements (e.g., particle image velocimetry and planar laser-induced fluorescence) at moderate to high Reynolds numbers, a T-shaped mixer was designed. It has a height of 4 centimetres, which is much larger than the dimensions of typically used micro-scale T-mixers (even a limited number of available macro-scale T-mixers) with the same geometry.

This paper aims to verify the previous flow regimes in literature and to validate our large-scale setup. Thus the paper is organized as follows. We first provide detailed descriptions of the experimental setup and the measuring technique. Further, experimental results are presented and previous experimental flow regimes are repeated, in which the Strouhal number of the unsteady flows is compared. Finally, the article is closed with a summary and outlook for future work.

Experimental setup and technique

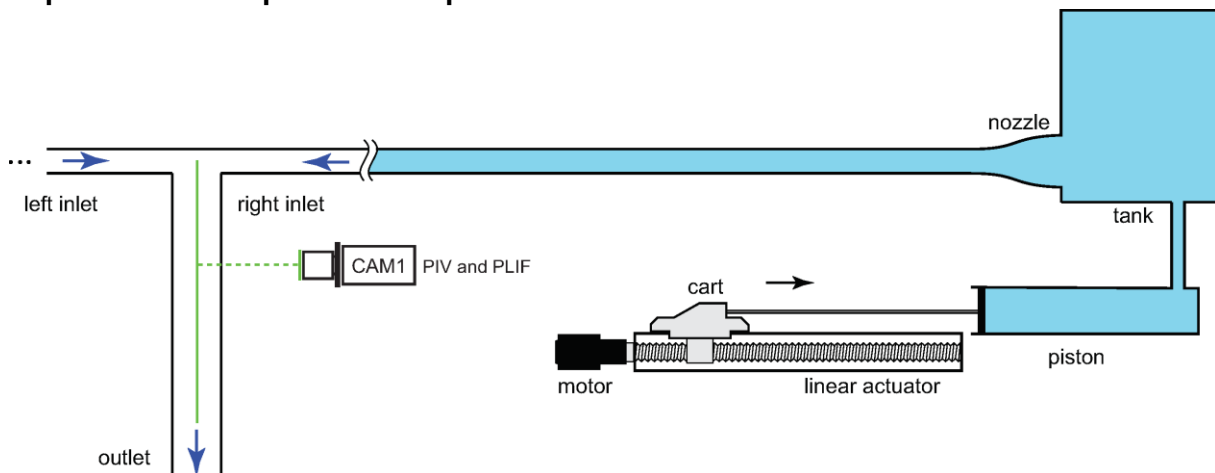


Figure 1. Sketch of the T-mixer setup, where the left branch is omitted (represented by three dots) to leave sufficient space for the details of the right-branch inlet. The setup consists of two symmetric branches and a T-junction section, where PIV measurements are taken. The arrows indicate the flow direction.

Figure 1 shows a schematic of the T-mixer setup. The working fluid is water at ambient temperature ($20\text{ }^{\circ}\text{C}$). The device is 6 m long and consists of two branches (inlet channels) of square cross-section $H = 40\text{ mm}$ with a length of 3 m ($75H$). The length of the inlet was chosen to allow fully laminar developed flow up to $Re = 650$ according to literature estimates. As reported in Shah and London (2014), the entrance length of a square duct for fully laminar developed flow was described as $L/H = C \cdot Re$, in which the coefficient C varies between 0.0328 and 0.09. The worse-case coefficient $C = 0.09$ yields an entrance length of $L \approx 59H$ for $Re = 650$. Thus, the inlet with a designed entrance length of $75H$ (3 m) is enough to obtain a fully developed laminar flow in our experimental setup. The outlet (main channel) of the T-mixer has a rectangular cross-section with dimensions of $2H \times H$ (width \times height), and it is $25H$ long. The flow rates at the two inlets are kept equal, and the mean speed U_0 (and hence the Reynolds number) are the same at the inlets and outlet channel because of the geometry.

For feasible manufacturing, the inlet channels of the T-mixer are made of several segments fabricated with acrylic glass (PMMA). Careful glueing of acrylic glass plates makes the square channels have a tolerance smaller than $\pm 0.25\text{ mm}$ for inlet width and height. Each segment channel has a length of 500 mm. They are connected through adapters and the connection parts are sealed with O-rings, polytetrafluoroethylene band and silicon. Note that the inner corners in the junction region are associated with small radii of curvature, measured smaller than 1 mm, which has negligible effects on flow behaviour (Thomas and Ameel. 2010). The outlet channel was also manufactured with the same procedure. The whole setup is supported by aluminium profiles for better operation and stability. During the assembly and experiments, the entire setup was carefully levelled using hydrodynamic equilibrium and the symmetry on both sides of the T junction was also ensured.

The fluid flow is driven at the two inlets by two pistons pushing at the same speed. The maximum output power of the servo motors is 570 W with a maximum rotation speed of 4980 RPM, which is precisely controlled via a National Instrument card and the software *IndraWorks* from Bosch-Rexroth company. The motors are connected to the end of the threaded shaft of the linear actuator, and the cart mounting on the actuator moves continuously, as shown in figure 1. Each piston is connected to the cart by a shaft and is driven to push the fluid with the desired flow rate. The outlet of each piston is connected to an acrylic tank through a rubber tube. These two equal-sized acrylic tanks have a dimension of $340\text{ mm} \times 340\text{ mm} \times 500\text{ mm}$, and they are

used to decay the fluid perturbations from the linear driving systems. The outlet of each tank is connected to the square-cross section inlet (in dimension $H \times H$) through a designed contraction nozzle.

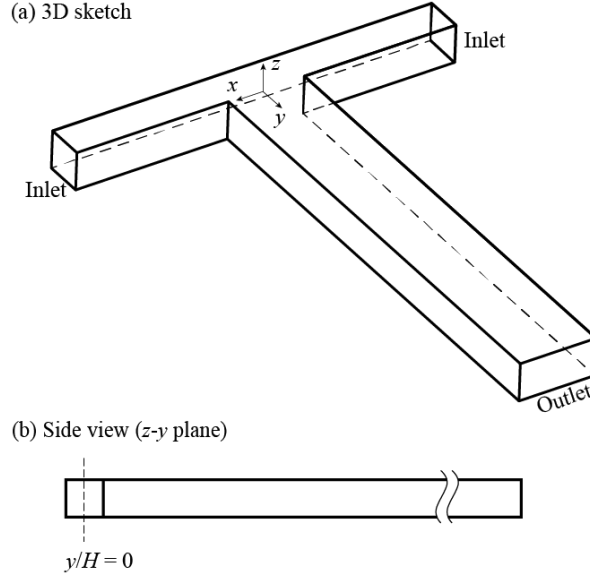


Figure 2. (a) A sketch of a T-junction section and coordinates. (b) The dashed line means the position where PIV measurements are taken.

Particle image velocimetry (PIV) was employed in the present setup for the velocity fields. PIV technique was used to measure the velocity field at a given location ($y/H = 0$) in the middle height of the outlet channel, see figure 2(b). A pulsed Nd:YAG laser system of 527-nm wavelength (DM50-527 Photonics) with a group of optics was used to generate a laser sheet to illuminate the flow. A 12-bit CMOS camera (Phantom VEO 640L, 2560×1600 pixel²) was applied to implement two-dimensional PIV measurements as well as image the flow. For PIV measurements, the whole setup was full of water seeded with 9-13 μm hollow glass spheres of specific gravity 1.03. Vector fields were processed from raw PIV images using LaVision Davis 10 PIV processing software. The multi-step algorithm is used with interrogation window 64×64 pixel² at the initial step reducing to the window 32×32 pixel² without overlap at the final step. The interrogation window at the final step includes approximate 7 dots for accurate displacement tracking. Machined hardware mounts were used to rigidly fix the camera and laser sheet orthogonally.

Results and discussion

Fully developed flow

The length of the inlets was designed to allow fully laminar developed flow up to $Re \leq 700$ according to literature estimates. For a square duct flow, the fully developed velocity profile is described as (Shah and London 2014; Chatwin and Sullivan 1982):

$$u = -\frac{4H^2}{\pi^3} \frac{dp}{\mu dx} \sum_{n=1,3,\dots}^{\infty} \frac{1}{n^3} (-1)^{\frac{n-1}{2}} \left[1 - \frac{\cosh(n\pi y/H)}{\cosh(n\pi/2)} \right] \cos\left(\frac{n\pi z}{H}\right), \quad (1)$$

where dp/dx is a pressure drop and μ is the dynamic viscosity of water. It can be derived as a function of the mean velocity U_0 , finding:

$$U_0 = -\frac{H^2}{12} \frac{dp}{\mu dx} \left[1 - \frac{192}{\pi^5} \sum_{n=1,3,\dots}^{\infty} \frac{1}{n^5} \tanh\left(\frac{n\pi}{2}\right) \right]. \quad (2)$$

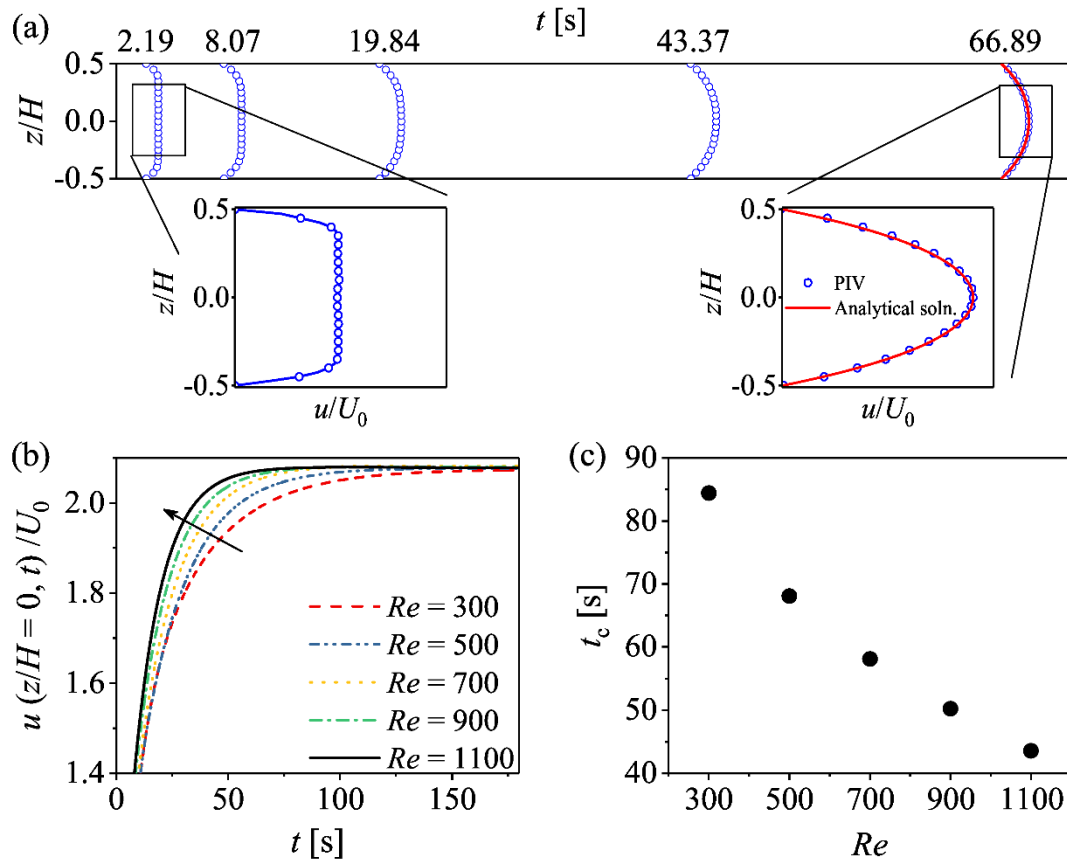


Figure 3. (a) Comparison of velocity profiles between PIV and analytical solution in the left inlet channel of the T-mixer at $Re = 700$ and $x/H = -2.5$. In the inset, the red solid line is the analytical velocity profile from the square duct flow Shah and London (2014) and the blue hollow circles denote the velocity profile from PIV results. (b) Comparison of centerline ($z/H = 0$) velocity normalized by the bulk mean velocity (U_0) versus developed time t for varying Reynolds numbers. The arrow indicates the direction of the curves' transition from $Re = 300$ to $Re = 1100$. (c) The critical developed time t_c when the centreline velocity reaches 98% of asymptotic steady state velocity.

In our setup, the fluid is driven by an imposed constant volume flux, note however that in the laminar regime the results are identical as for fluid driven at a constant pressure drop (e.g., Chaudhury et al. 2015). To check the fully developed laminar flow of the present setup, the PIV technique is employed in both inlet channels. The measurement is taken in the upstream positions with a distance $2.5H$ to the centre of the T-mixer to avoid the effects of the flows at the T-mixer on the velocity profiles. Figure 3(a) demonstrates the velocity profiles of an inlet channel when $Re = 700$. Our measurement results are in very good agreement with corresponding theoretical velocity flow profiles (equation 1 in a square duct, see the inset in figure 3a). When the centerline velocity reaches 98% of asymptotic steady state velocity, here, the flow is defined to reach a fully developed state (Chaudhury et al. 2015). These results indicate that the entrance length can guarantee a fully developed laminar flow with $Re \leq 1100$ and the entrance length can be written as $L/H = 0.07Re$. Besides, the centerline velocities for different Reynolds numbers are shown in figure 3(b). The required time for each flow to reach asymptotic steady state velocity decreases monotonically as the Reynolds number increases. A similar varying trend was also reported in a pipe flow (Chaudhury et al. 2015). To guide the experiments below, the critical development times for different Reynolds numbers are extracted and shown in figure 3(c). According to these findings, we started the following experiments when the fully developed laminar flow was achieved.

Flow regimes when $Re < 400$

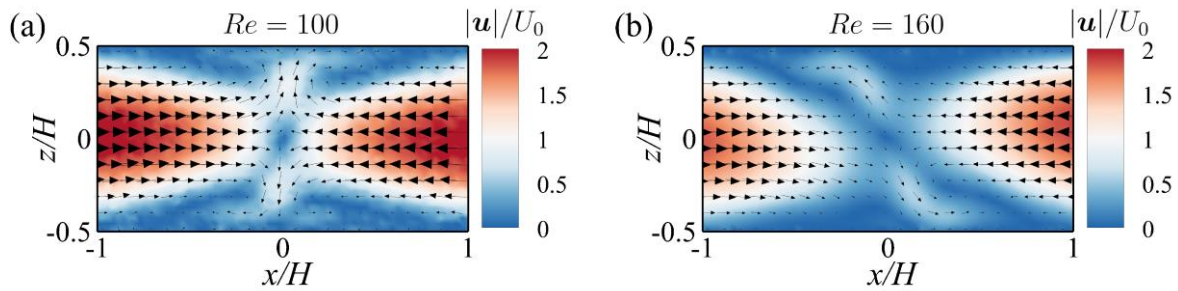


Figure 4. The velocity field from PIV results when (a) $Re = 100$ and (b) $Re = 160$.

When $Re = 100$, flows are left-right, top-down and accordingly the four vortices are approximately symmetric, as shown in the PIV results in figure 4(a). After a long-time running of the experiments, the flow pattern in this range gradually becomes slightly asymmetric, which is due to thermal convection effects. Because the room temperature is not uniform in space and has a difference from the water temperature, in the present large-scale setup, it gives rise to a weak thermal convection circulation and then affects the flow regimes in the T junction. The studies of this effect are less reported in previous experimental studies because of their small-scale setups, leading to much smaller Grashof numbers. The physics and effects of the thermal convection on T-mixer flows are worth to be investigated further and in future experiments, the temperature will be controlled by e.g. homogenizing the air in the room. We find that for $Re > 110$, the engulfment flow emerges, which includes both steady and unsteady asymmetric flows. For example, in figure 4(b), two counterclockwise rotating vortices were observed. During the experimental time, these two vortices remain approximately steady. In different experimental trials, the two vortices are equally likely to occur clockwise and counterclockwise, which was already observed in Thomas and Ameel. (2010) and confirms that the setup was built to high accuracy, thus preserving the spatial symmetries of the system.

With the increase of Re , the flow pattern becomes unsteady (periodic). Figure 5 shows the velocity field at a different time in a period when $Re = 280$. This regime is characterized by a periodic shear-layer process at the fluid interface. In the beginning, two vortices are gradually formed at the left-upper and right-low corners (see figure 5a). Subsequently, two vortices slowly roll along with the inter-fluid interface, and engulf each other in the centre of the channel figure 5(b), before the process begins again (a).

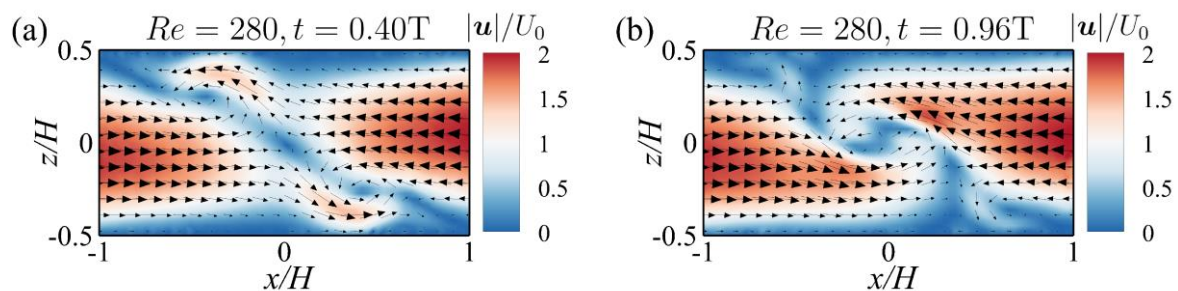


Figure 5. The velocity field from PIV results at a different time when $Re = 280$: (a) $t = 0.40T$; (b) $t = 0.96T$.

For $300 < Re < 340$, both periodic unsteady engulfment flow and unsteady symmetric flow can occur, but the likelihood of unsteady symmetric flow increases with increasing Re . For $Re > 340$ almost all realizations yield symmetric flow but with quasi-periodic temporal dynamics. Figure 6 shows the velocity field for PIV results when $Re = 360$. In the figure, four vortices (clockwise and counterclockwise) stay in the symmetric position leftward and rightward. At a

different time, these four vortices move quasi-periodically around their positions at the top and bottom walls, resulting in the centerline of the two streams also tilting along with the time rather than being strictly vertical. As Re increases, this topology is less likely to be maintained and instantaneously the degree of asymmetry increases as the flow becomes chaotic. Note that when the time average is taken, the left-right and top-bottom symmetries are recovered in this regime (in contrast to the chaotic engulfment regime, which only retains a central symmetry in average).

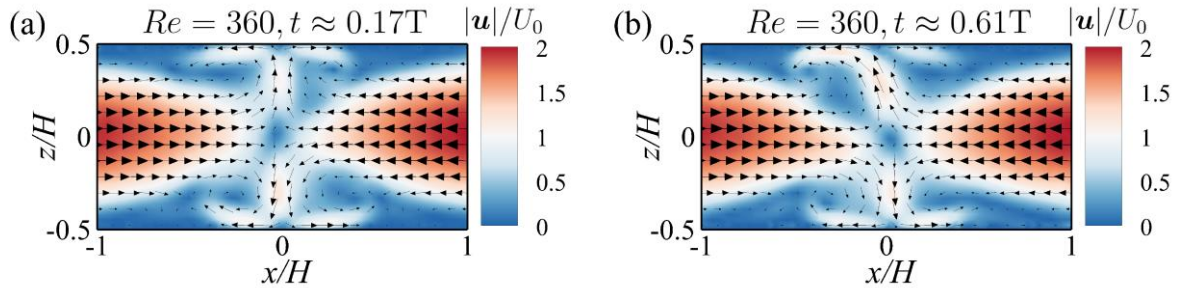


Figure 6. The velocity field from PIV results at a different time when $Re = 360$: (a) $t \approx 0.17T$; (b) $t \approx 0.61T$. The oscillation periodicity is approximately extracted.

The frequency f of the periodic and quasi-periodic flow, expressed with the dimensionless Strouhal number (St), can be compared to the present study by computing $St = fH/U_0$. In order to quantify periodicity for unsteady flows in the present study, the velocity magnitude $|u|$ between frame k and frame $k + 1$ (where k is from 2 to the total number of image frames), was correlated to that between image frame 1 and frame 2 using

$$R(k) = 1 - \frac{1}{M \times N} \sum_{m=1}^M \sum_{n=1}^N (|u|_1(m, n) - |u|_k(m, n))^2, \quad (3)$$

where M and N are the number of the velocity vectors along x and z directions, respectively. Equation (3) is similar to one of the image correlation algorithms, named the Minimum Quadratic Difference method (Gui and Merzkirch 2000). The correlation coefficient along time is plotted in figure 7(a), in which the periodicity can be observed in 14 advect time units (defined as $t_{adv} = H/U_0$). As shown in figure 7(b), between $Re = 300$ and 340 there is a sharp change of the Strouhal number, which was attributed to the onset of the symmetric flow. Our experimental results are in agreement with those of Schikarski et al. (2017): as the flow becomes asymmetric and chaotic, it becomes difficult to extract the main oscillation frequency and longer experimental runs would be necessary.

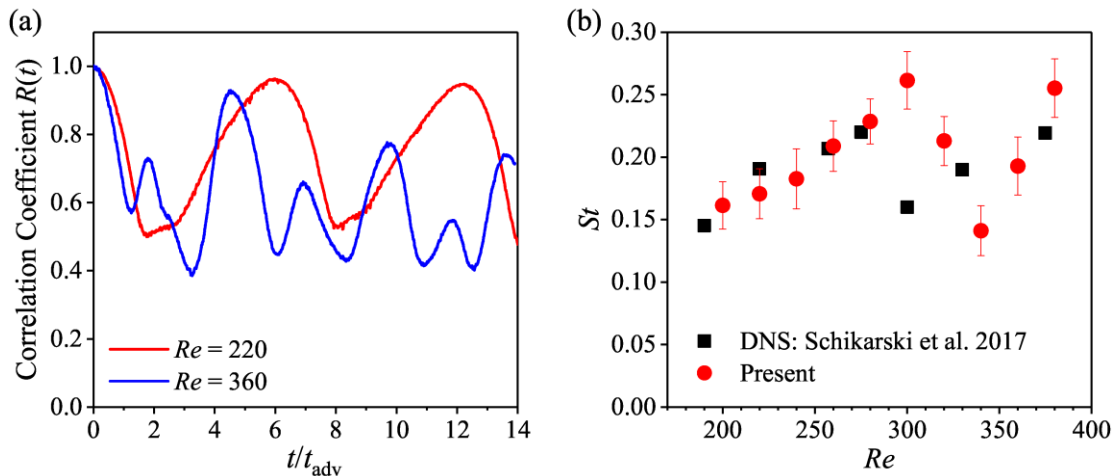


Figure 7. (a) The time correlation of the velocity magnitude when $Re = 220$ and 360 . (b) Strouhal number as a function of Reynolds number. The data from the simulations of Schikarski et al. (2017) are shown as black circles.

Summary

In this study, we designed a large-scale T-mixer with a height of 4 centimetres, which is beyond the dimensions of mostly used micro-scale T-mixers in the same geometry. The PIV technique is used in this setup with long inlets. And we found that with carefully operations, the present setup can achieve the inlets with fully developed laminar flows when $Re \leq 1100$ and reproduce the flow regimes in previous studies with the exact same geometry. But due to the channel height of 4 centimetres, thermal convection can influence the flow regimes during the experiments. In the next, the whole setup will be improved with adjustments (e.g., isolation between the setup and room, homogenization of the air in the room) to avoid this effect. Finally, planar laser-induced fluorescence will be performed and the scaling of mixing down to the Batchelor scale will be measured.

Acknowledgements

H. Li gratefully acknowledges the support from the Chinese Scholarship Council (No. CSC201804930530). This work was supported by the Deutsche Forschungsgemeinschaft (DFG, German Science Foundation) - INST 144/464.

Reference

- Thomas, S., Ameel, T.A., 2010:** "An Experimental Investigation of Moderate Reynolds Number Flow in a T-Channel", *Experiments in Fluids*, 49(6), pp.1231-1245
- Thomas, S., Ameel, T.A., Guilkey, J., 2010:** "Mixing Kinematics of Moderate Reynolds Number Flows in a T-channel", *Physics of Fluids*, 22(1), pp. 013601
- Hoffmann, M., Schlüter, M., Rübiger, N., 2006:** "Experimental Investigation of Liquid-liquid Mixing in T-shaped Micro-mixers Using μ -LIF and μ -PIV", *Chemical Engineering Science*, 61(9), pp. 2968-2976
- Fani, A., Camarri, S., Salvetti, M.V. 2013:** "Investigation of the Steady Engulfment Regime in a Three-dimensional T-mixer", *Physics of Fluids*, 25(6), pp. 064102.
- Fani, A., Camarri, S., Salvetti, M.V., 2014:** "Unsteady Asymmetric Engulfment Regime in a T-mixer", *Physics of Fluids*, 26(7), pp. 074101
- Camarri, S., Mariotti, A., Galletti, C., Brunazzi, E., Mauri, R., Salvetti, M.V. 2020:** "An Overview of Flow Features and Mixing in Micro T and Arrow Mixers", *Industrial & Engineering Chemistry Research*, 59(9), pp. 3669-3686
- Engler, M., Kockmann, N., Kiefer, T., Woias, P., 2004:** "Numerical and Experimental Investigations on Liquid Mixing in Static Micromixers", *Chemical Engineering Journal*, 101(1-3), pp. 315-322
- Schikarski, T., Peukert, W., Avila, M., 2017:** "Direct Numerical Simulation of Water-ethanol Flows in a T-mixer", *Chemical Engineering Journal*, 324, pp. 168-181
- Minakov, A., Rudyak, V., Dekterev, A., Gavrilov, A., 2013:** Investigation of Slip Boundary Conditions in the T-shaped Microchannel. *International Journal of Heat and Fluid Flow*, 43, pp. 161-169
- Schikarski, T., Trzenschiok, H., Peukert, W., Avila, M., 2019:** "Inflow Boundary Conditions Determine T-mixer Efficiency", *Reaction Chemistry & Engineering*, 4(3), pp. 559-568
- Zhang, J.W., Liu, S.F., Cheng, C., Li, W.F., Xu, X.L., Liu, H.F., Wang, F.C., 2019:** "Investigation of Three-dimensional Flow Regime and Mixing Characteristic in T-jet Reactor", *Chemical Engineering Journal*, 358, pp. 1561-1573
- Poole, R., Alfateh, M., Gauntlett, A., 2013:** "Bifurcation in a T-channel junction: Effects of aspect ratio and shear-thinning", *Chemical Engineering Science*, 104, pp. 839-848
- Shah, R.K., London, A.L., 2014:** "Laminar flow forced convection in ducts: a source book for compact heat exchanger analytical data", Academic press
- Soleymani, A., Yousefi, H., Turunen, I., 2008:** "Dimensionless number for identification of flow patterns inside a T-micromixer", *Chemical Engineering Science*, 63(21), pp. 5291-5297
- Chaudhury, R.A., Herrmann, M., Frakes, D.H., Adrian, R.J., 2015:** "Length and time for development of laminar flow in tubes following a step increase of volume flux", *Experiments in Fluids*, 56(1), pp. 1-10

Cherlo, S.K.R., Pushpavanam, S., 2010: "Effect of depth on onset of engulfment in rectangular micro-channels", *Chemical Engineering Science*, 65(24), pp. 6486–6490

Chatwin, P.C., Sullivan, P.J., 1982: "The effect of aspect ratio on longitudinal diffusivity in rectangular channels", *Journal of Fluid Mechanics*, 120, pp. 347–358

Gui, L., Merzkirch, W., 2000: "A comparative study of the MQD method and several correlation-based PIV evaluation algorithms", *Experiments in Fluids*, 28, pp. 36–44